# Measurement of $K^- p$ radiative capture to $\gamma\Lambda$ and $\gamma\Sigma^0$ for $p_{K^-}$ between 514 and 750 MeV/$c$

S. Prakhov,[1,*] P. Vancraeyveld,[2,†] N. Phaisangittisakul,[1] B. M. K. Nefkens,[1] V. Bekrenev,[3] W. J. Briscoe,[4] L. De Cruz,[2]
D. Isenhower,[5] N. Knecht,[6,‡] A. Koulbardis,[3] N. Kozlenko,[3] S. Kruglov,[3] G. Lolos,[6] I. Lopatin,[3] A. Marušić,[1,§] S. McDonald,[1,‖]
Z. Papandreou,[6] D. Peaslee,[7,¶] J. W. Price,[1] J. Ryckebusch,[2] M. Sadler,[5] A. Shafi,[4] A. Starostin,[1] H. M. Staudenmaier,[8]
I. I. Strakovsky,[4] I. Supek,[9] and T. Van Cauteren[2]

[1]*University of California Los Angeles, Los Angeles, California 90095-1547, USA*
[2]*Ghent University, B-9000 Ghent, Belgium*
[3]*Petersburg Nuclear Physics Institute, Gatchina 188350, Russia*
[4]*The George Washington University, Washington, DC 20052-0001, USA*
[5]*Abilene Christian University, Abilene, Texas 79699-7963, USA*
[6]*University of Regina, Saskatchewan S4S OA2, Canada*
[7]*University of Maryland, College Park, Maryland 20742-4111, USA*
[8]*Universität Karlsruhe, Karlsruhe D-76128, Germany*
[9]*Rudjer Boskovic Institute, HR-10000 Zagreb, Croatia*

Differential cross sections for $K^-$ radiative capture in flight on the proton, leading to the $\gamma\Lambda$ and $\gamma\Sigma^0$ final states, have been measured at eight $K^-$ momenta between 514 and 750 MeV/$c$. The data were obtained with the Crystal Ball multiphoton spectrometer installed at the separated $K/\pi$ beam line C6 of the BNL Alternating Gradient Synchrotron. The results substantially improve the existing experimental data available for studying radiative decays of excited hyperon states. An exploratory theoretical analysis is performed within the Regge-plus-resonance approach. According to this analysis, the $\gamma\Sigma^0$ final state is dominated by hyperon-resonance exchange and hints at an important role for a resonance in the mass region of 1700 MeV. In the $\gamma\Lambda$ final state, in contrast, the resonant contributions account for only half the strength, and the data suggest the importance of a resonance in the mass region of 1550 MeV.

## I. INTRODUCTION

The experimental study of the radiative reactions $K^- p \to \gamma\Lambda$ and $K^- p \to \gamma\Sigma^0$ is of special interest because these reactions are among the very few cases in which information about the radiative decays of hyperon resonances can be obtained. Measuring the properties of these resonances constitutes important input to models that attempt to describe the internal structure of hadrons. The Particle Data Group's Review of Particle Physics (RPP) [1] lists a number of established $\Lambda$ and $\Sigma$ resonances (see Table I), albeit with large uncertainties in the masses, widths, and branching ratios. So far, sufficient experimental data and many models exist for the radiative capture of kaons at rest (see Refs. [2,3] and references therein), which is dominated by the $\Lambda(1405)S_{01}$ resonance. A more comprehensive study of the hyperon spectrum is possible through the study of in-flight capture of kaons by a proton, for which only a meager data set is available. To date, no dedicated

model calculations exist for this reaction channel. Through crossing symmetry [4–8], the radiative capture process is intimately related to kaon photoproduction, which is better studied experimentally and theoretically.

In contrast to kaon photoproduction, the measurement of the radiative capture in flight requires a photon spectrometer and careful subtraction of the large background from single $\pi^0$ production. An experimental study of the reactions $K^- p \to$ neutrals became feasible with the Crystal Ball (CB) multiphoton spectrometer installed at the separated $K/\pi$ beam line C6 of the BNL Alternating Gradient Synchrotron (AGS). Besides the radiative processes, this study also involved the measurement of the following final states: $\eta\Lambda$, $\bar{K}^0 n$, $\pi^0\Lambda$, $\pi^0\Sigma^0$, $\pi^0\pi^0\Lambda$, $\pi^0\pi^0\Sigma^0$, and $\pi^0\pi^0\pi^0\Lambda$, reported in Refs. [9–13]. A reliable measurement of the radiative reactions would not be possible without the extensive measurement of most of these reactions.

In the present work, we report on the first measurement of the differential cross sections for the radiative reactions $K^- p \to \gamma\Lambda$ and $K^- p \to \gamma\Sigma^0$ at eight incident $K^-$ momenta between 514 and 750 MeV/$c$. An exploratory theoretical analysis is performed within the Regge-plus-resonance approach [14–17]. Many experimental details have already been presented in Ref. [9] and are omitted in this paper. The preliminary results for the radiative reaction $K^- p \to \gamma\Lambda$ with many experimental details are given in Ref. [18]. An independent analysis of the $K^- p \to \gamma\Sigma^0$ reaction, using the same data set, was recently presented in Ref. [19], in which the authors report total cross sections or their upper limits only.

_____

*prakhov@ucla.edu

†pieter.vancraeyveld@ugent.be

‡Present address: Physics Department of University of Toronto, 60 St. George St., Toronto, Ontario M5S 1A7, Canada.

§Present address: Collider Accelerator Department, Brookhaven National Laboratory, Upton, New York 11973, USA.

‖Present address: TRIUMF, 4004 Wesbrook Mall, Vancouver, British Columbia V6T 2A3, Canada.

¶Deceased.

TABLE I. Selection of established $\Lambda$ and $\Sigma$ resonances relevant to the data presented in the present work. We list the resonances' mass and total decay width ranges as given in the RPP [1], in addition to their star status. In the last two columns, we tabulate predictions by the Bonn constituent-quark model [20,21] for the partial electromagnetic decay widths to the ground-state $\Lambda(1116)$ and $\Sigma^0(1193)$.

| Resonance | $L_{I \cdot 2J}$ | status | Mass (MeV) | Width (MeV) | $\Gamma_{\Lambda\gamma}$ (MeV) | $\Gamma_{\Sigma^0\gamma}$ (MeV) |
|---|---|---|---|---|---|---|
| $\Lambda(1520)$ | $D_{03}$ | $****$ | $1519.5 \pm 1.0$ | $15.6 \pm 1.0$ | 0.258 | 0.157 |
| $\Lambda(1600)$ | $P_{01}$ | $***$ | 1560–1700 | 50–250 | 0.104 | 0.0679 |
| $\Sigma(1660)$ | $P_{11}$ | $***$ | 1630–1690 | 50–70 | 0.451 | 0.578 |
| $\Lambda(1670)$ | $S_{01}$ | $****$ | 1660–1680 | 25–50 | $0.159 \times 10^{-3}$ | 3.827 |
| $\Sigma(1670)$ | $D_{13}$ | $****$ | 1665–1685 | 40–80 | 1.457 | 0.214 |
| $\Lambda(1690)$ | $D_{03}$ | $****$ | 1685–1695 | 50–70 | 0.0815 | 1.049 |

## II. EXPERIMENTAL SETUP

The experimental study was performed with the Crystal Ball multiphoton spectrometer, which is a highly segmented sphere made of NaI(Tl). The CB consists of 672 almost identical crystals packed in two hermetically sealed and evacuated hemispheres. The solid angle covered by the CB is 93% of $4\pi$ sr. The crystals have the shape of a truncated triangular pyramid, all pointed toward the center of the CB. The crystal length is 40.6 cm, which corresponds to 15.7 radiation lengths. The typical energy resolution for electromagnetic showers in the CB was $\Delta E/E = 0.020/(E[\text{GeV}])^{0.36}$. The directions of the photon showers were measured with a resolution in $\theta$ (the polar angle with respect to the beam axis) of $\sigma_\theta = 2°$–$3°$. The resolution in azimuthal angle $\phi$ is $\sigma_\theta / \sin\theta$.

The C6 line of the AGS provided a beam of negative kaons and pions with the $K^-/\pi^-$ ratio enhanced to about 0.1 by two electrostatic separators. The beam particles were incident on a 10-cm-long liquid-hydrogen (LH$_2$) target located in the center of the Crystal Ball. The momentum resolution $\sigma_p/p$ for an individual incident kaon varied from 0.6% to 1.%, depending on the momentum value. The mean value $p_{K^-}$ for the incident-momentum spectra and the momentum spread $\delta_p$, which were determined at the target center, are listed in Table II. The uncertainty in determining the mean beam momentum is 2–3 MeV/$c$.

The LH$_2$ target was surrounded by a 16-cm-diameter pipe made of four thin scintillation counters that functioned as a veto for the beam interactions with charged particles in the final state. The 120-cm length of the veto counters ensured almost 100% rejection of those events. The 5-mm thickness of the counters implied both a good efficiency in vetoing charged particles and a low probability for photon conversion.

## III. DATA HANDLING

Since the Crystal Ball detector is designed as a multiphoton spectrometer, $K^-p$ interactions were studied by measuring the photons and, when possible, the neutron in the final state. The $\Lambda$ and $\Sigma^0$ hyperons were measured in the CB via the decay chains $\Lambda \to \pi^0 n \to 2\gamma n$ and $\Sigma^0 \to \gamma\Lambda \to \gamma\pi^0 n \to 3\gamma n$. As the final-state photons produce electromagnetic showers in the NaI(Tl) crystals, they can be recognized as so-called clusters in the density of the energy deposited in the CB. The outgoing neutrons can also be detected if the products of their interactions in the NaI(Tl) material produce enough ionization to form a cluster. In general, a cluster in the CB is defined as a group of neighboring crystals in which energy is deposited from the interaction of a photon, a charged particle, or a neutron produced in the final state. The software threshold for the cluster energy was chosen to be 20 MeV; this value optimizes the yield of the reconstructed events for the $K^-p \to$ neutrals processes.

The kinematic-fitting technique was used to select candidates for the radiative reactions that were studied. Those candidates were selected by testing the following hypotheses:

$$K^-p \to \gamma\Lambda \to \gamma\pi^0 n \to 3\gamma n, \tag{1}$$

$$K^-p \to \gamma\Sigma^0 \to \gamma\gamma\Lambda \to \gamma\gamma\pi^0 n \to 4\gamma n. \tag{2}$$

The incident kaon was parametrized in the kinematic fit by the five measured variables: momentum, angles $\theta_x$ and $\theta_y$, and position coordinates $x$ and $y$ at the target. A photon cluster was parametrized by the three measured variables: energy and angles $\theta$ and $\phi$. As the data were taken with a 10-cm-long LH$_2$ target, the $z$ coordinate of the vertex was a free variable of the kinematic fit. Including $z$ into the fit

TABLE II. Number of the initial candidates, $N_{\text{Cand}}$, for the radiative reactions $K^-p \to \gamma\Lambda$ and $K^-p \to \gamma\Sigma^0$ and the events, $N_{\text{Evnt}}$, left after the background subtraction for the eight beam momenta. The last two rows list the corresponding numbers for $K^-p \to \gamma\Sigma^0$ as reported in Ref. [19].

| $p_{K^-} \pm \delta_p$ (MeV/$c$) | $514 \pm 10$ | $560 \pm 11$ | $581 \pm 12$ | $629 \pm 11$ | $659 \pm 12$ | $687 \pm 11$ | $714 \pm 11$ | $750 \pm 13$ |
|---|---|---|---|---|---|---|---|---|
| $N_{\text{Cand}}(K^-p \to \gamma\Lambda)$ | 567 | 1103 | 1691 | 1785 | 1836 | 2099 | 2273 | 3456 |
| $N_{\text{Evnt}}(K^-p \to \gamma\Lambda)$ | 140 | 236 | 301 | 454 | 344 | 453 | 491 | 739 |
| $N_{\text{Cand}}(K^-p \to \gamma\Sigma^0)$ | 249 | 486 | 751 | 838 | 977 | 1226 | 1331 | 2407 |
| $N_{\text{Evnt}}(K^-p \to \gamma\Sigma^0)$ | 67 | 130 | 248 | 319 | 339 | 430 | 581 | 1120 |
| $N_{\text{Cand}}(K^-p \to \gamma\Sigma^0)$, Ref. [19] | 35 | 87 | 139 | 216 | 234 | 383 | 576 | 647 |
| $N_{\text{Evnt}}(K^-p \to \gamma\Sigma^0)$, Ref. [19] | 1 | 8 | 4 | 33 | 10 | 33 | 196 | 214 |

improves the angular resolution in the photon directions. When the final-state neutron was not detected, its energy and two angles were free variables of the fit. For the neutron detected in the CB, the angles of its cluster were used as the measured variables, while the neutron energy was a free variable of the fit. Since all reactions in our analysis had a particle decaying in flight, the decay length of this particle was also a free variable of the kinematic fit. The corresponding secondary vertex is then determined by the primary-vertex coordinates, the direction of the decaying particle, and the decay length.

The candidates for reaction (1) were searched for in three- and four-cluster events. The three-cluster events were tested for the case when only the three photons were detected in the CB. The four-cluster events were tested for the case in which all four final-state particles were detected. Similarly, the candidates for reaction (2), which have four photons and a neutron in the final state, were searched for in four- and five-cluster events. The test of each hypothesis involved all possible permutations of assigning the detected clusters to the particles in the reaction chain. The events for which at least one permutation satisfied the tested hypothesis at the 5% confidence level, CL (i.e., with a probability larger than 5%), were accepted as the reaction candidates. The permutation with the largest CL was used to reconstruct the kinematics of the reaction.

The candidates selected for the two radiative reactions are contaminated with background events that have to be subtracted from the experimental distributions. The first source of the background events appears from processes that are not kaon interactions in the LH$_2$ target. The major fraction of these interactions are $K^-$ decays in the beam. This background was investigated using the data taken when the target was empty. The fraction of this background in our event candidates was determined from the ratio of the total number of the beam kaons incident on the full target to the corresponding number for the empty target. The fraction of the so-called empty-target background, remaining in the radiative-reaction candidates after all selection cuts, is at the level of 15%–22%. The properly weighted empty-target spectra were subtracted from the full-target distributions before the acceptance correction of the latter. The second source of the background events appears from the following processes:

$$K^- p \rightarrow K^0_S n \rightarrow \pi^0 \pi^0 n \rightarrow 4\gamma n, \qquad (3)$$

$$K^- p \rightarrow \pi^0 \Lambda \rightarrow \pi^0 \pi^0 n \rightarrow 4\gamma n, \qquad (4)$$

$$K^- p \rightarrow \pi^0 \Sigma^0 \rightarrow \pi^0 \gamma \Lambda \rightarrow \pi^0 \gamma \pi^0 n \rightarrow 5\gamma n, \qquad (5)$$

which can be misidentified as the radiative reactions when some of the final-state photons are not detected in the CB. Our measurement of these three reactions is given in detail in Ref. [9]. Based on the results from Ref. [9], the background from each of the three reactions can be understood via a Monte Carlo simulation.

A Monte Carlo (MC) simulation of reactions (1) and (2) was used to determine their acceptance. Based on the MC simulation of reactions (3), (4), and (5), their remaining backgrounds were subtracted from the radiative-reaction candidates. Reactions (1) and (2) were simulated with an isotropic production-angle distribution. Reactions (3), (4), and (5) were simulated according to their differential cross sections

measured using the same data [9]. The MC events of each beam momentum were then propagated through a full GEANT (version 3.21) simulation of the CB detector, folded with the CB resolutions and trigger conditions, and analyzed the same way as the experimental data. The small difference between the experimental data and the MC simulation for the neutron response in the CB was not important, as we summed the events with and without the neutron detected.

The analysis of the MC simulation for the background reactions showed that $\pi^0 \Lambda$ events cause the largest contamination of the $\gamma \Lambda$ candidates. This occurs when one photon from the decay of the outgoing $\pi^0$ is not detected in the CB. Similarly, $\pi^0 \Sigma^0$ events constitute the largest contamination of the $\gamma \Sigma^0$ candidates. In four- and five-cluster events, the background from reactions (3), (4), and (5) was partially suppressed by the 2% CL cut on the hypotheses of these reactions themselves; that is, all events that satisfied these hypotheses with probability larger than 2% were rejected. Further suppression of the remaining background events can be done by tightening the cut on the CL of the hypotheses used to select the radiative-reaction candidates. However, this leads to decreasing statistics. The MC spectra with the remaining background from reactions (3), (4), and (5) were then subtracted from the experimental distributions with the radiative candidates. The normalization of the spectra for the subtraction was based on the ratio between the number of the simulated events for the background reactions to the number of the experimental events found for those reactions themselves in the data (see Ref. [9] for details).

The acceptance for both reactions $K^- p \rightarrow \gamma \Lambda$ and $K^- p \rightarrow \gamma \Sigma^0$ was determined as a function of $\cos \theta^*$, where $\theta^*$ is the production angle of the outgoing photon (i.e., the angle between the direction of the outgoing photon and the incident $K^-$ meson) in the center-of-mass (c.m.) frame. The acceptance for both the radiative reactions is shown in Fig. 1 for two beam momenta: 514 and 750 MeV/$c$. These acceptances include the effects of all our standard cuts used in the event selection. A poorer $\cos \theta^*$ acceptance of the forward $\theta^*$ angles for a higher beam momentum is mostly due to the larger threshold on the CB total energy in the event trigger. This threshold was 0.9 GeV for $p_{K^-} = 514$ MeV/$c$ and became 1.5 GeV for $p_{K^-} = 750$ MeV/$c$.

## IV. EXPERIMENTAL RESULTS AND THEIR INTERPRETATION

The number of the radiative-reaction candidates initially selected with our standard cuts and the number of the experimental events left after the background subtraction are listed in Table II for our two radiative reactions at the eight beam momenta. The comparison of these numbers reflects the fraction of the background events that were subtracted from the reaction candidates.

The differential cross sections are given as a function of $\cos \theta^*$, where the full range from $-1$ to 1 is divided into 12 bins. Since the $K^- p \rightarrow \gamma \Lambda$ reaction for the four highest beam momenta has very low acceptance in the last bin, the results for this bin are not presented. To calculate cross
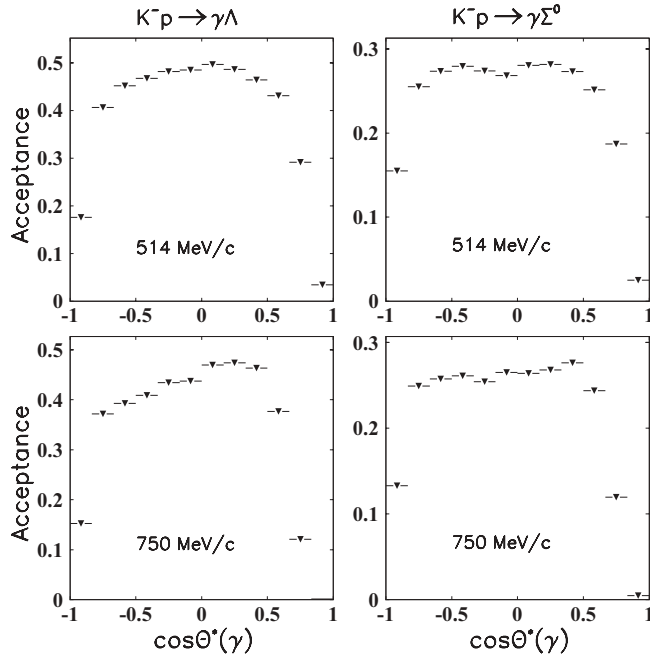
FIG. 1. Acceptance for the production angle $\theta^*$ of the outgoing photon in the c.m. frame for the reactions $K^- p \to \gamma \Lambda$ and $K^- p \to \gamma \Sigma^0$ at beam momenta of 514 and 750 MeV/$c$.

sections, the Particle Data Group (PDG) [1] branching ratio $0.358 \pm 0.005$ for the $\Lambda \to \pi^0 n$ decay was used. The effective proton density in the target times the effective target length was $(4.05 \pm 0.08) \times 10^{-7}$ $\mu$b$^{-1}$. The calculation of the total number of beam kaons incident on the target is given in detail in Ref. [18]. The uncertainties presented in our results for the differential cross sections are statistical only.

The systematic uncertainty that includes the evaluation of the losses of good events resulting from pileup clusters and the uncertainty in the total number of beam kaons incident on the target is about 7%. This uncertainty is the same for all $K^- p \to$ neutrals reactions and has been determined in the earlier analyses of the data [9]. Another systematic uncertainty comes from the subtraction of large backgrounds from other

reactions, the shapes and contributions of which are based on the MC simulation of those reactions. This uncertainty was estimated by varying the kinematic-fit CL value used for event selection, where a tighter cut on the CL leads to a better ratio of the signal to the background. In addition to our standard 5%-CL cut, 10% and 20% cuts were also tested. All results agreed within the statistical uncertainties. The largest fluctuations were observed in the first and the last bins, which have the smallest acceptance. No preferred trend of the results to smaller or larger values after tightening the CL cut was observed. Our conservative value for this type of systematic uncertainty is 7%. All imperfections in the shapes of our differential cross sections can be explained by statistical fluctuations. Adding our two systematic uncertainties in quadrature gives 10% for our total systematic uncertainty; it is not included in the errors presented in the tables and figures with our results.

Our differential cross sections for $K^- p \to \gamma \Lambda$ as a function of $\cos \theta^*$ for the outgoing photon are given for each of the eight beam momenta in Tables III and IV. The corresponding results for $K^- p \to \gamma \Sigma^0$ are given in Tables V and VI. Because of our limited statistics and the subtraction of the large backgrounds, several points resulted in unphysical negative values; however, all of them are consistent with positive values within their uncertainties.

In Figs. 2 and 3, we show the Legendre polynomial fits to our differential cross sections,

$$d\sigma/d\Omega = \sum_{l=0}^{l_{max}} A_l P_l(\cos \theta^*), \qquad (6)$$

where $P_l$ is the Legendre polynomial of order $l$, and $A_l$ is its coefficient. The choice of the maximum order $l_{max}$ was limited by our statistics: It was 1 for the three lowest beam momenta of the $K^- p \to \gamma \Sigma^0$ reaction and 2 for all other fits. The results of Legendre polynomial fits are given for both the reactions in Tables VII and VIII.

To interpret our results for the radiative reactions $K^- p \to \gamma \Lambda$ and $K^- p \to \gamma \Sigma^0$, we compared them with Regge-plus-resonance (RPR) model calculations. The RPR approach has been developed to describe photo-induced and electro-induced kaon production off protons [14–17]. The $p(\gamma, K)Y$

TABLE III. Differential cross sections for the $K^- p \to \gamma \Lambda$ reaction for the four lowest beam momenta.

| $p_{K^-}$ (MeV/$c$) | $514 \pm 10$ | $560 \pm 11$ | $581 \pm 12$ | $629 \pm 11$ |
| $\cos \theta_\gamma^*$ | $d\sigma/d\Omega$ ($\mu$b/sr) | $d\sigma/d\Omega$ ($\mu$b/sr) | $d\sigma/d\Omega$ ($\mu$b/sr) | $d\sigma/d\Omega$ ($\mu$b/sr) |
| --- | --- | --- | --- | --- |
| $-0.917$ | $18.7 \pm 11.3$ | $10.4 \pm 8.2$ | $3.2 \pm 11.1$ | $7.7 \pm 4.8$ |
| $-0.750$ | $9.1 \pm 4.0$ | $1.2 \pm 3.2$ | $3.9 \pm 3.8$ | $6.6 \pm 2.2$ |
| $-0.583$ | $1.8 \pm 2.1$ | $3.1 \pm 2.3$ | $4.4 \pm 2.2$ | $5.0 \pm 1.6$ |
| $-0.417$ | $3.6 \pm 2.5$ | $2.1 \pm 2.2$ | $4.6 \pm 1.9$ | $3.6 \pm 1.6$ |
| $-0.250$ | $4.2 \pm 2.8$ | $4.5 \pm 1.9$ | $4.3 \pm 2.1$ | $3.1 \pm 1.7$ |
| $-0.083$ | $7.8 \pm 3.3$ | $4.4 \pm 2.1$ | $2.0 \pm 1.8$ | $4.3 \pm 1.6$ |
| $0.083$ | $-2.2 \pm 3.5$ | $6.6 \pm 2.8$ | $5.7 \pm 2.2$ | $4.1 \pm 1.7$ |
| $0.250$ | $4.5 \pm 3.8$ | $3.3 \pm 2.9$ | $6.4 \pm 3.4$ | $6.9 \pm 1.9$ |
| $0.417$ | $1.2 \pm 4.0$ | $2.3 \pm 3.7$ | $-0.2 \pm 4.3$ | $6.9 \pm 2.2$ |
| $0.583$ | $11.8 \pm 4.5$ | $9.1 \pm 3.5$ | $7.2 \pm 3.9$ | $5.6 \pm 2.6$ |
| $0.750$ | $12.4 \pm 5.6$ | $13.8 \pm 4.1$ | $7.6 \pm 4.2$ | $10.5 \pm 3.1$ |
| $0.917$ | $23.5 \pm 21.6$ | $18.9 \pm 16.5$ | $3.6 \pm 19.9$ | $15.9 \pm 9.5$ |

TABLE IV. Differential cross sections for the $K^- p \to \gamma \Lambda$ reaction for the four highest beam momenta.

| $p_{K^-}$ (MeV/$c$) $\cos \theta_\gamma^*$ | $659 \pm 12$ $d\sigma/d\Omega$ ($\mu$b/sr) | $687 \pm 11$ $d\sigma/d\Omega$ ($\mu$b/sr) | $714 \pm 11$ $d\sigma/d\Omega$ ($\mu$b/sr) | $750 \pm 13$ $d\sigma/d\Omega$ ($\mu$b/sr) |
|---|---|---|---|---|
| $-0.917$ | $0.9 \pm 5.1$ | $4.8 \pm 5.5$ | $9.1 \pm 4.4$ | $5.3 \pm 4.2$ |
| $-0.750$ | $4.9 \pm 1.9$ | $1.9 \pm 2.7$ | $2.9 \pm 2.1$ | $4.2 \pm 1.6$ |
| $-0.583$ | $1.4 \pm 1.7$ | $9.7 \pm 2.0$ | $2.9 \pm 1.8$ | $5.0 \pm 1.5$ |
| $-0.417$ | $5.3 \pm 1.7$ | $6.6 \pm 1.7$ | $6.4 \pm 1.6$ | $6.6 \pm 1.3$ |
| $-0.250$ | $3.4 \pm 1.4$ | $5.2 \pm 1.6$ | $3.4 \pm 1.4$ | $2.1 \pm 1.1$ |
| $-0.083$ | $3.0 \pm 1.5$ | $1.8 \pm 1.8$ | $4.3 \pm 1.3$ | $4.6 \pm 1.2$ |
| $0.083$ | $2.0 \pm 1.5$ | $4.3 \pm 1.7$ | $6.4 \pm 1.4$ | $3.8 \pm 1.0$ |
| $0.250$ | $1.4 \pm 1.9$ | $7.1 \pm 1.9$ | $4.9 \pm 1.6$ | $3.9 \pm 1.2$ |
| $0.417$ | $4.2 \pm 2.2$ | $5.7 \pm 2.1$ | $3.0 \pm 2.0$ | $4.2 \pm 1.5$ |
| $0.583$ | $7.6 \pm 2.3$ | $0.0 \pm 2.9$ | $4.2 \pm 2.2$ | $4.7 \pm 1.8$ |
| $0.750$ | $11.2 \pm 3.6$ | $7.5 \pm 5.6$ | $9.9 \pm 4.2$ | $8.9 \pm 3.8$ |
| $0.917$ | $-$ | $-$ | $-$ | $-$ |

amplitude, which is dominated by nonresonant $t$-channel contributions, is modeled in terms of $K^+(494)$ and $K^{*+}(892)$ Regge-trajectory exchange. For the $p(\gamma, K^+)\Lambda$ reaction, the best model is coined Regge-2. In $K\Sigma$ photoproduction two equivalent Regge models are available. A recent analysis of $n(\gamma, K^+)\Sigma^-$ data allowed us to isolate an optimal model, coined Regge-3. The Regge-model amplitudes can be supplemented with a selection of $s$-channel resonance diagrams. Since the radiative kaon-capture reaction is related to photo-induced kaon production through crossing symmetry, the amplitude for the kaon-capture process can be obtained by analytic continuation of the kaon-production amplitude in which the signs of the kaon and photon momenta are reversed. Crossing symmetry interchanges the roles of the Mandelstam $s$ and $u$ variables. The Mandelstam $t$ variable remains the same, as do the contributions to the amplitude that arise from $t$-channel exchange. Therefore, one can apply the Regge model, developed for kaon photoproduction, to the description of radiative kaon capture, without introducing or adjusting any parameters [8]. As can be appreciated in Fig. 4, the Regge-model predictions (solid lines) for $K^- p \to \gamma \Lambda$ are of the same order as the measured differential cross sections and are in reasonable agreement with the data except for an

underprediction of the strength at forward angles. The situation for the $K^- p \to \gamma \Sigma^0$ channel is entirely different. One can see in Fig. 5 that the Regge model underpredicts the data by an order of magnitude. This hints at an important role for resonance-exchange terms in the reaction amplitude.

To assess the possible resonant contributions to the radiative capture reactions, the Regge-model amplitudes can be enriched with hyperon-resonance exchange terms, along similar lines as $s$-channel resonances have been added for the $p(\gamma, K)Y$ processes [14,15]. Table I lists six established hyperon resonances relevant to the energy range of the data presented here. Owing to the lack of experimental data for the electromagnetic decay widths of these resonances, we have included predictions by the Bonn constituent-quark model [20,21]. When fixing the resonances' mass and width at the central RPP value, inclusion of a spin-1/2 or spin-3/2 resonance introduces two or three free parameters, respectively.[1] The quality and amount of the differential-cross-section data

_____

[1]The most general Lagrangian for spin-3/2 resonances has three additional degrees of freedom, often called *off-shell* parameters. To limit the total number of fitting parameters, we discard the latter.

TABLE V. Differential cross sections for the $K^- p \to \gamma \Sigma^0$ reaction for the four lowest beam momenta.

| $p_{K^-}$ (MeV/$c$) $\cos \theta_\gamma^*$ | $514 \pm 10$ $d\sigma/d\Omega$ ($\mu$b/sr) | $560 \pm 11$ $d\sigma/d\Omega$ ($\mu$b/sr) | $581 \pm 12$ $d\sigma/d\Omega$ ($\mu$b/sr) | $629 \pm 11$ $d\sigma/d\Omega$ ($\mu$b/sr) |
|---|---|---|---|---|
| $-0.917$ | $-2.2 \pm 8.4$ | $2.2 \pm 6.4$ | $4.8 \pm 6.3$ | $4.8 \pm 3.5$ |
| $-0.750$ | $11.0 \pm 4.1$ | $-0.6 \pm 3.9$ | $1.6 \pm 2.8$ | $7.4 \pm 2.2$ |
| $-0.583$ | $2.6 \pm 4.0$ | $0.9 \pm 2.7$ | $1.9 \pm 2.6$ | $2.0 \pm 2.3$ |
| $-0.417$ | $6.4 \pm 3.8$ | $3.0 \pm 2.2$ | $3.5 \pm 1.9$ | $6.2 \pm 1.7$ |
| $-0.250$ | $7.9 \pm 3.8$ | $9.3 \pm 2.7$ | $10.5 \pm 2.2$ | $4.3 \pm 1.7$ |
| $-0.083$ | $3.4 \pm 3.5$ | $4.9 \pm 2.4$ | $9.5 \pm 2.1$ | $5.7 \pm 1.6$ |
| $0.083$ | $0.5 \pm 3.6$ | $6.8 \pm 3.1$ | $7.6 \pm 2.7$ | $7.8 \pm 2.2$ |
| $0.250$ | $8.8 \pm 4.2$ | $8.7 \pm 3.5$ | $1.7 \pm 4.2$ | $8.1 \pm 2.4$ |
| $0.417$ | $1.3 \pm 4.5$ | $5.3 \pm 3.1$ | $4.8 \pm 4.4$ | $7.2 \pm 2.6$ |
| $0.583$ | $5.1 \pm 5.1$ | $4.8 \pm 4.5$ | $13.5 \pm 4.0$ | $12.5 \pm 2.3$ |
| $0.750$ | $-0.4 \pm 5.5$ | $3.8 \pm 3.5$ | $5.5 \pm 3.2$ | $3.3 \pm 3.2$ |
| $0.917$ | $17.2 \pm 13.2$ | $-0.8 \pm 15.9$ | $19.8 \pm 9.9$ | $8.4 \pm 6.9$ |

TABLE VI. Differential cross sections for the $K^- p \to \gamma \Sigma^0$ reaction for the four highest beam momenta.

| $p_{K^-}$ (MeV/$c$) $\cos \theta_\gamma^*$ | $659 \pm 12$ $d\sigma/d\Omega$ ($\mu$b/sr) | $687 \pm 11$ $d\sigma/d\Omega$ ($\mu$b/sr) | $714 \pm 11$ $d\sigma/d\Omega$ ($\mu$b/sr) | $750 \pm 13$ $d\sigma/d\Omega$ ($\mu$b/sr) |
|---|---|---|---|---|
| $-0.917$ | $3.8 \pm 4.3$ | $-2.1 \pm 7.5$ | $9.9 \pm 3.8$ | $11.1 \pm 3.8$ |
| $-0.750$ | $3.2 \pm 2.1$ | $6.1 \pm 2.5$ | $4.9 \pm 2.1$ | $10.4 \pm 1.9$ |
| $-0.583$ | $5.1 \pm 2.0$ | $4.8 \pm 2.3$ | $6.9 \pm 1.8$ | $5.9 \pm 1.6$ |
| $-0.417$ | $6.3 \pm 1.8$ | $6.1 \pm 2.1$ | $8.3 \pm 1.8$ | $10.5 \pm 1.3$ |
| $-0.250$ | $6.1 \pm 1.9$ | $4.4 \pm 2.0$ | $8.8 \pm 1.6$ | $12.1 \pm 1.4$ |
| $-0.083$ | $6.2 \pm 1.8$ | $6.4 \pm 2.5$ | $8.1 \pm 1.8$ | $9.8 \pm 1.5$ |
| $0.083$ | $5.4 \pm 2.1$ | $10.1 \pm 1.9$ | $6.5 \pm 2.1$ | $8.6 \pm 1.7$ |
| $0.250$ | $7.0 \pm 2.3$ | $9.1 \pm 3.2$ | $6.9 \pm 2.3$ | $12.8 \pm 2.1$ |
| $0.417$ | $6.1 \pm 2.7$ | $14.8 \pm 3.1$ | $14.2 \pm 2.2$ | $12.2 \pm 2.3$ |
| $0.583$ | $9.8 \pm 2.6$ | $7.7 \pm 3.7$ | $10.7 \pm 2.4$ | $10.7 \pm 2.5$ |
| $0.750$ | $6.8 \pm 2.0$ | $8.3 \pm 3.7$ | $17.1 \pm 3.4$ | $18.4 \pm 3.0$ |
| $0.917$ | $22.1 \pm 10.8$ | $6.9 \pm 8.2$ | $5.6 \pm 12.5$ | $22.0 \pm 12.9$ |

presented here are not sufficient to perform fits with multiple resonances. Therefore, we carried out fits with a single resonance at a time. For the $K^- p \to \gamma \Lambda$ channel, we obtain a typical $\chi^2$ value of 115 for 92 data points. Five of the six fits for the $K^- p \to \gamma \Sigma^0$ reaction attain $\chi^2$ of 230 for 96 data points, except for the fit including $\Lambda(1670) S_{01}$, which converged at a $\chi^2$ value of 355 for 96 data points.

In Fig. 4, we show the $K^- p \to \gamma \Lambda$ model calculations including the $\Lambda(1520) D_{03}$, $\Sigma(1660) P_{11}$, or $\Sigma(1670) D_{13}$ state, since, according to the Bonn model, these resonances have the largest branching ratio to the $\gamma \Lambda$ channel. The strength of the $\Sigma(1660) P_{11}$ and $\Sigma(1670) D_{13}$ resonances increases with the energy of the incoming kaon, whereas the $\Lambda(1520) D_{03}$ contribution is more uniformly spread. The angular dependence of these three models are in reasonable agreement with our data. Figure 5 features model calculations for the $K^- p \to \gamma \Sigma^0$ channel including the $\Lambda(1600) P_{01}$, $\Lambda(1670) S_{01}$, or $\Lambda(1690) D_{03}$ resonance. The angular dependencies of $\Lambda(1600) P_{01}$ and $\Lambda(1670) S_{01}$ are similar, but the strength of the $\Lambda(1600) P_{01}$ contribution is much more uniform as a function

of the beam energy. The angular dependence of $\Lambda(1690) D_{03}$ has a trend opposite to $\Lambda(1600) P_{01}$ and $\Lambda(1670) S_{01}$ and better matches the experimental data at the highest momenta.

The evaluation of the total cross sections for the radiative reactions $K^- p \to \gamma \Lambda$ and $K^- p \to \gamma \Sigma^0$ was based on the Legendre polynomial fits shown in Figs. 2 and 3. The results obtained for both radiative reactions are listed for each of the eight beam momenta in Table IX and are also shown in Fig. 6 in conjunction with the RPR model calculations. We assume that the systematic uncertainties in our values for the total cross sections have the same magnitude as for the differential cross sections. These systematic uncertainties are not included in the presented results.

For the $K^- p \to \gamma \Lambda$ reaction, the total cross section falls off as the center-of-mass energy $W$ rises. This trend is predicted by the Regge model, which accounts for roughly half the strength. The addition of the $\Lambda(1520) D_{03}$ resonance allows us to largely make up for the missing strength. The Bonn constituent-quark model also predicts a large electromagnetic decay width for the transitions of $\Sigma(1660) P_{11}$ and $\Sigma(1670) D_{13}$
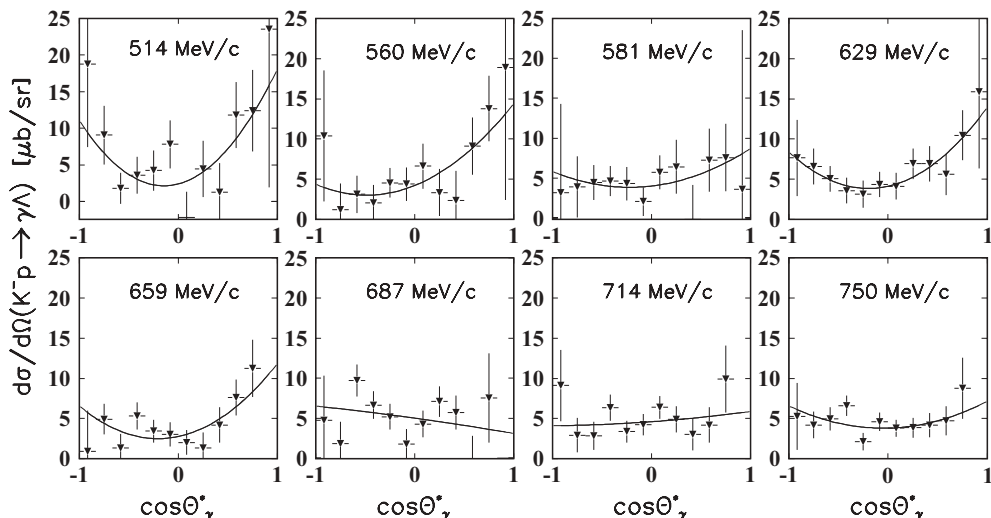


FIG. 2. Our differential cross sections for $K^- p \to \gamma \Lambda$ at the eight beam momenta. The curves are the Legendre polynomial fits to our data.
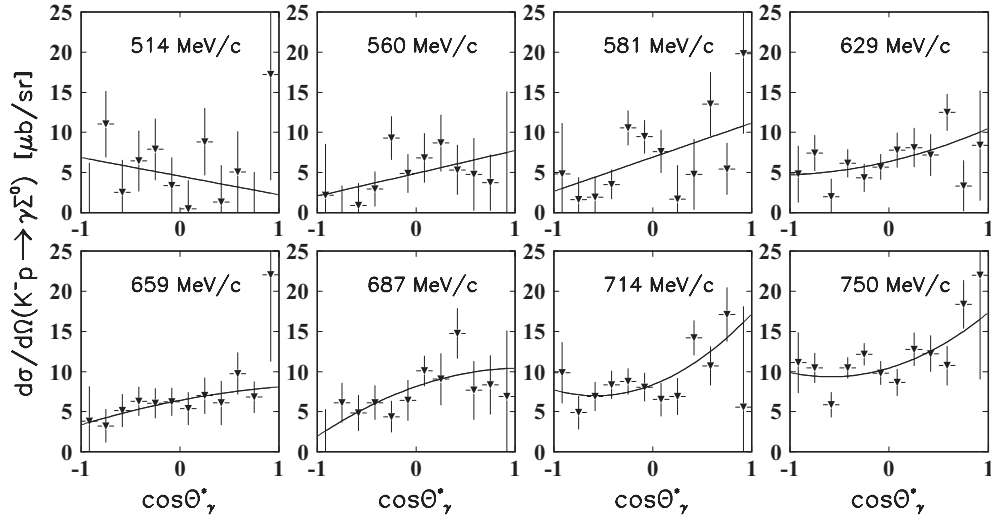
FIG. 3. Our differential cross sections for $K^- p \to \gamma \Sigma^0$ at the eight beam momenta. The curves are the Legendre polynomial fits to our data.

to $\Lambda(1116)\gamma$. The RPR fit including any of these two resonances improves the description of the total cross section at the highest energy bins, but it fails to account for the rise at lower energies. In the $K^- p \to \gamma \Sigma^0$ reaction channel, the energy dependence of the total cross section differs notably from the $\gamma \Lambda$ final state, peaking in the highest measured energy bin. This behavior is opposite to the Regge-model result, which underestimates the total cross section by a factor of 4 and predicts a falloff as energy increases. A nice correspondence with the data at lower energies is realized through the inclusion of the $\Lambda(1600)P_{01}$ resonance, which has a particularly large value for the total decay width in the RPP. The Regge-model calculations supplemented with either the $\Lambda(1670)S_{01}$ resonance or $\Lambda(1670)S_{01}$, having a large value for $\Gamma_{\gamma \Sigma^0}$ in the Bonn model, allow us to reproduce the apparent peak in the total cross section data, but they fail at lower energies. For both reaction channels presented in this work, the data cannot be understood in terms of a reaction amplitude consisting of nonresonant terms in conjunction with a single resonance. The energy dependence of the total cross sections, however, suggests a prominent contribution from a

resonance in the range of 1550 MeV for the $\gamma \Lambda$ final state and of 1700 MeV for $\gamma \Sigma^0$.

## V. COMPARISON WITH OTHER RESULTS

Our results for $K^- p \to \gamma \Lambda$ in flight are unique and at the moment can be compared to theoretical predictions only. For the $K^- p \to \gamma \Sigma^0$ reaction, there is also an independent analysis of the same data set, resulting only in the determination of the total cross sections [19]. That analysis was conducted by the Valparaiso-Argonne (V-A) group and published before the present analysis became available. We now believe that the V-A analysis has been published prematurely because the comparison of the two analyses (see Fig. 7) reveals that the V-A results for the total cross sections are systematically lower than ours. The magnitude of the disagreement between the two analyses cannot be evaluated accurately because of the inadequate treatment of the systematic uncertainties in the V-A analysis. Moreover, for half of the V-A cross sections, only upper limits were reported. Those upper limits are based on the statistical uncertainties only and the confidence level at which they have been determined is omitted in

TABLE VII. Legendre polynomial coefficients for the $K^- p \to \gamma \Lambda$ reaction at the eight beam momenta.

| $p_{K^-}$ (MeV/$c$) | $A_0$ | $A_1$ | $A_2$ | $\chi^2$/ndf[a] |
|---|---|---|---|---|
| 514 ± 10 | 6.45 ± 1.39 | 3.49 ± 2.51 | 8.11 ± 3.87 | 1.13 |
| 560 ± 11 | 5.94 ± 1.12 | 5.01 ± 2.07 | 3.44 ± 2.91 | 0.59 |
| 581 ± 12 | 5.08 ± 1.21 | 1.44 ± 2.17 | 2.18 ± 3.05 | 0.43 |
| 629 ± 11 | 6.46 ± 0.78 | 2.77 ± 1.46 | 4.68 ± 2.05 | 0.27 |
| 659 ± 12 | 4.90 ± 0.80 | 2.61 ± 1.48 | 4.29 ± 2.06 | 1.04 |
| 687 ± 11 | 4.95 ± 1.00 | −1.70 ± 1.79 | −0.14 ± 2.62 | 1.83 |
| 714 ± 11 | 4.74 ± 0.81 | 0.89 ± 1.49 | 0.25 ± 2.07 | 1.03 |
| 750 ± 13 | 4.83 ± 0.67 | 0.30 ± 1.21 | 2.03 ± 1.72 | 1.01 |

[a]ndf = number of degrees of freedom.

TABLE VIII. Legendre polynomial coefficients for the $K^- p \to \gamma \Sigma^0$ reaction at the eight beam momenta.

| $p_{K^-}$ (MeV/$c$) | $A_0$ | $A_1$ | $A_2$ | $\chi^2$/ndf |
|---|---|---|---|---|
| 514 ± 10 | 4.55 ± 1.30 | −2.32 ± 2.81 | – | 0.83 |
| 560 ± 11 | 4.90 ± 0.95 | 2.84 ± 2.11 | – | 0.75 |
| 581 ± 12 | 6.91 ± 0.89 | 4.26 ± 1.93 | – | 1.59 |
| 629 ± 11 | 6.78 ± 0.78 | 2.88 ± 1.49 | 0.81 ± 1.96 | 1.25 |
| 659 ± 12 | 6.18 ± 0.71 | 2.36 ± 1.34 | −0.46 ± 1.90 | 0.42 |
| 687 ± 11 | 7.49 ± 0.98 | 4.24 ± 1.85 | −1.31 ± 2.53 | 0.84 |
| 714 ± 11 | 9.72 ± 0.79 | 4.73 ± 1.51 | 2.73 ± 2.09 | 1.07 |
| 750 ± 13 | 11.50 ± 0.75 | 3.72 ± 1.40 | 2.11 ± 1.89 | 1.55 |

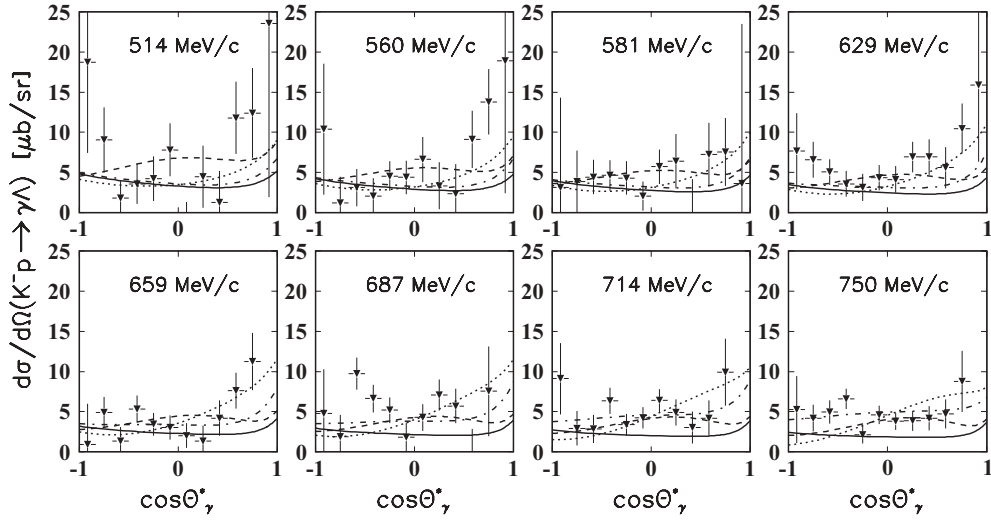FIG. 4. Comparison of our differential cross sections for $K^- p \to \gamma \Lambda$ with RPR model calculations. The solid line is the Regge-2 model prediction consisting solely of nonresonant diagrams. The dashed, dotted, and dashed-dotted curves represent fits to our data of the Regge-2 model supplemented with the $\Lambda(1520)D_{03}$, $\Sigma(1660)P_{11}$, or $\Sigma(1670)D_{13}$ resonance, respectively.

Ref. [19]. Our total cross sections are plotted in Fig. 7 after adding linearly our statistical and systematic uncertainties.

The difference between our total cross sections and the V-A ones is of the same order of magnitude (50–75 $\mu$b) for all beam momenta. Such a feature is indicative of the oversubtraction of the large background contributions in the V-A analysis. At our energies, the yield of the major background reactions ($K^- p \to \pi^0 \Sigma^0$ and $K^- p \to \pi^0 \Lambda$) is almost the same as a function of beam momentum [9]. Then a wrong normalization of these background contributions should result in such a deviation from the actual cross section, the magnitude of which is similar at each momentum. According to the authors of Ref. [19], the normalization of the MC simulations for the background reactions was based on their total cross sections. However, it

is not clear how such a normalization is possible if the total cross sections for $K^- p \to \gamma \Sigma^0$ have not yet been determined. In our opinion, the approach used in Ref. [19] to normalize the contributions from the background reactions led to their substantial oversubtraction.

Another feature of the V-A analysis that should result in large systematic uncertainties is the use of very tight selection cuts to improve the signal-to-background ratio. To illustrate the consequences of applying such tight cuts, we list the numbers of the events selected in each of the two analyses in Table II for comparison. The corresponding numbers of the events selected in the V-A analysis are many times smaller than ours. Besides leading to poor statistics, the use of tight selection cuts requires excellent agreement between
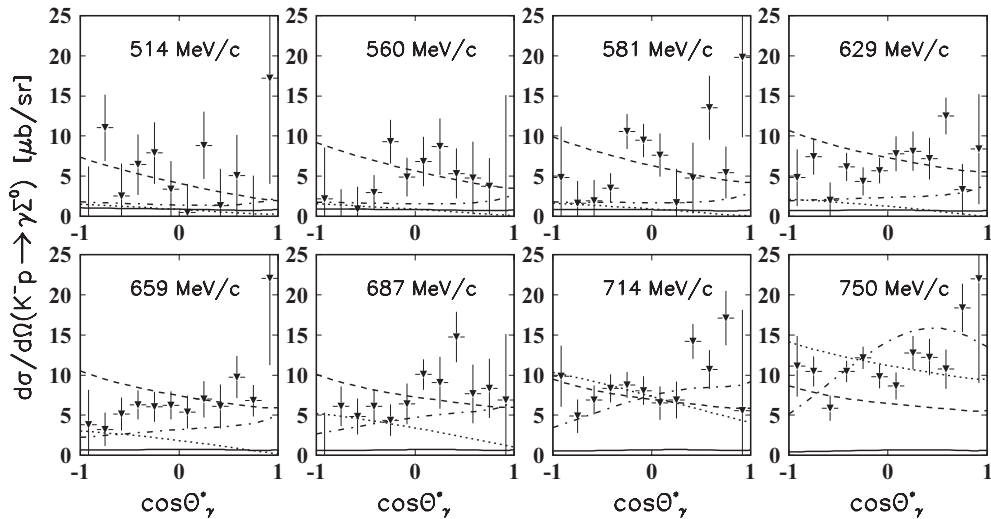


FIG. 5. Comparison of our differential cross sections for $K^- p \to \gamma \Sigma^0$ with RPR model calculations. The solid line is the Regge-3 model prediction consisting solely of nonresonant diagrams. The dashed, dotted, and dashed-dotted curves represent fits to our data of the Regge-3 model supplemented with the $\Lambda(1600)P_{01}$, $\Lambda(1670)S_{01}$, or $\Lambda(1690)D_{03}$ resonance, respectively.

TABLE IX. The total cross sections for the radiative reactions $K^- p \to \gamma \Lambda$ and $K^- p \to \gamma \Sigma^0$ at the eight beam momenta.

| $p_{K^-}$ (MeV/$c$) | $514 \pm 10$ | $560 \pm 11$ | $581 \pm 12$ | $629 \pm 11$ | $659 \pm 12$ | $687 \pm 11$ | $714 \pm 11$ | $750 \pm 13$ |
|---|---|---|---|---|---|---|---|---|
| $W$ (MeV) | $1569 \pm 4$ | $1589 \pm 5$ | $1598 \pm 5$ | $1620 \pm 5$ | $1634 \pm 5$ | $1647 \pm 5$ | $1659 \pm 5$ | $1676 \pm 6$ |
| $\sigma_{\gamma \Lambda}$ ($\mu$b) | $81 \pm 23$ | $75 \pm 19$ | $64 \pm 30$ | $81 \pm 13$ | $62 \pm 11$ | $62 \pm 12$ | $60 \pm 8$ | $61 \pm 8$ |
| $\sigma_{\gamma \Sigma^0}$ ($\mu$b) | $57 \pm 19$ | $62 \pm 25$ | $87 \pm 16$ | $85 \pm 12$ | $78 \pm 12$ | $94 \pm 16$ | $122 \pm 17$ | $144 \pm 15$ |

the experimental data and the MC simulations for both the signal and background reactions. Besides knowing the reaction dynamics, this agreement assumes that the MC simulation reproduces correctly the experimental resolutions and the trigger conditions. In our opinion, such an agreement was not sufficiently illustrated in Ref. [19], especially for the $\chi^2$-type function $F$ used for the selection of $K^- p \to \gamma \Sigma^0$ candidates. As all variances $1/w$, which reflect the experimental resolution of each term in the function $F$, have been determined from the MC simulation, it does not mean that they are correct for the experimental data.
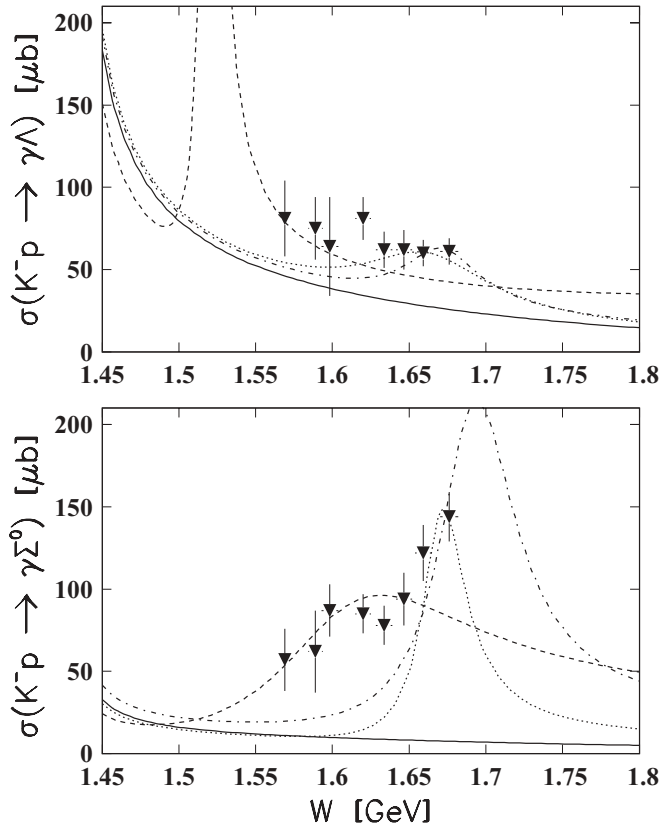


FIG. 6. Our total cross sections as a function of the center-of-mass energy $W$ for $K^- p \to \gamma \Lambda$ (top) and $K^- p \to \gamma \Sigma^0$ (bottom). The solid lines are the Regge-2 model prediction for $K^- p \to \gamma \Lambda$ (top) and the Regge-3 model prediction for $K^- p \to \gamma \Sigma^0$ (bottom). The dashed, dotted, and dashed-dotted curves shown for $K^- p \to \gamma \Lambda$ represent the Regge-2 model supplemented with the $\Lambda(1520)D_{03}$, $\Sigma(1660)P_{11}$, or $\Sigma(1670)D_{13}$ resonance, respectively. The dashed, dotted, and dashed-dotted curves shown for $K^- p \to \gamma \Sigma^0$ represent the Regge-3 model supplemented with the $\Lambda(1600)P_{01}$, $\Lambda(1670)S_{01}$, or $\Lambda(1690)D_{03}$ resonance, respectively.

The sensitivity of the results to the cuts being applied is tested in the V-A analysis by adding those cuts one by one. Most of those cuts just duplicate one of the terms of their function $F$. It seems that instead it would be more reasonable to tighten only the cut on the magnitude of $F$ for improving the signal-to-background ratio and testing the sensitivity of the results to that.

The systematic uncertainties reported in Ref. [19] are, in our opinion, significantly underestimated, since neither the effect from very tight cuts nor the effect from the subtraction of large background contributions were taken into account. The overall 10% systematics uncertainty borrowed from the V-A analysis of the $K^- p \to \pi^0 \Sigma^0$ reaction [22] definitely does not take those effects into account. The systematic uncertainty in the acceptance owing to a possible deviation of the $K^- p \to \gamma \Sigma^0$ differential cross sections from the isotropic distribution was estimated in Ref. [19] as +20%. This shows the strong sensitivity of the V-A results to the reaction dynamics. However, the approach used for that in Ref. [19] needs a better justification. The statistics available in the V-A analysis at the beam momentum of 750 MeV/$c$ was sufficient for the determination of their own $K^- p \to \gamma \Sigma^0$ differential cross section. Then the difference between their standard method and the result obtained by the integration of the differential cross section would allow a better estimate of this type of systematic uncertainty.
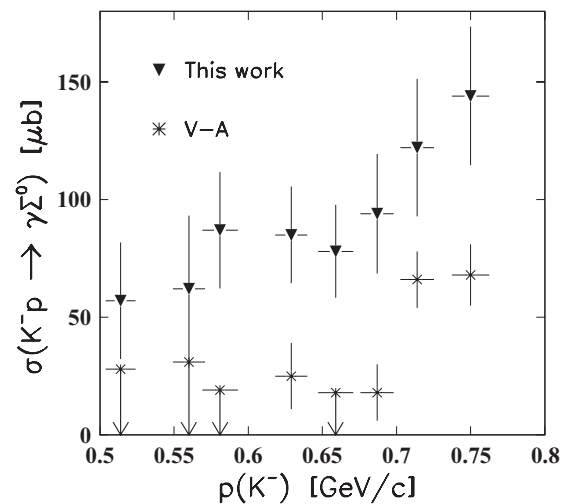


FIG. 7. Our $K^- p \to \gamma \Sigma^0$ total cross sections as a function of the beam momentum compared to the V-A results from Ref. [19]. The uncertainties plotted for our results are the sum of statistical and systematic uncertainties. The uncertainties plotted for V-A results are statistical only. The V-A points shown by arrows are upper limits.

## VI. SUMMARY

For the first time, the differential cross sections for $K^-$ radiative capture in flight on the proton, leading to the $\gamma\Lambda$ and $\gamma\Sigma^0$ final states, have been measured at eight $K^-$ momenta between 514 and 750 MeV/$c$. The data were obtained with the Crystal Ball multiphoton spectrometer installed at the separated $K/\pi$ beam line C6 of the BNL Alternating Gradient Synchrotron. The results substantially improve the existing experimental data available for studying radiative decays of excited hyperon states. An exploratory theoretical analysis is performed within the Regge-plus-resonance approach keeping fixed the nonresonant contributions to the reaction amplitude, optimized against kaon photoproduction data. According to this analysis, the $K^-p \to \gamma\Sigma^0$ reaction is dominated by hyperon-resonance exchange and hints at an important role for a resonance in the mass region of 1700 MeV. For the $K^-p \to \gamma\Lambda$ reaction, however, the resonant contributions account for only half the strength, and the data suggest the importance of a resonance in the mass region of 1550 MeV.

In our opinion, the analysis of the $K^-p \to \gamma\Sigma^0$ reaction reported in Ref. [19] was conducted with serious shortcomings, and we do not recommend those results to be used. The discrepancy between the V-A results and ours cannot be evaluated accurately for lack of the adequate systematic uncertainties in the V-A analysis.

[1] C. Amsler *et al.* (Particle Data Group), Phys. Lett. B **667**, 1 (2008).

[2] D. A. Whitehouse *et al.*, Phys. Rev. Lett. **63**, 1352 (1989).

[3] P. B. Siegel and B. Saghai, Phys. Rev. C **52**, 392 (1995).

[4] C. R. Ji and S. R. Cotanch, Phys. Rev. C **38**, 2691 (1988).

[5] R. Williams, C.-R. Ji, and S. R. Cotanch, Phys. Rev. D **41**, 1449 (1990).

[6] R. A. Williams, C.-R. Ji, and S. R. Cotanch, Phys. Rev. C **43**, 452 (1991).

[7] J. C. David, C. Fayard, G. H. Lamot, and B. Saghai, Phys. Rev. C **53**, 2613 (1996).

[8] T. Van Cauteren, P. Vancraeyveld, and J. Ryckebusch, *Hyperon Resonances in Radiative Kaon Capture*, Acta Physica Polonica B Proceedings Supplement, Proceedings of Excited QCD, Zakopane, Poland, 2009, Vol. 2, Number 2 (Jagiellonian Univ., Poland, 2009), pp. 347–352.

[9] S. Prakhov *et al.*, Phys. Rev. C **80**, 025204 (2009).

[10] A. Starostin *et al.*, Phys. Rev. C **64**, 055205 (2001).

[11] S. Prakhov *et al.*, Phys. Rev. C **69**, 042202 (2004).

[12] S. Prakhov *et al.*, Phys. Rev. C **70**, 034605 (2004).

[13] M. Borgh *et al.*, Phys. Rev. C **68**, 015206 (2003).

[14] T. Corthals, J. Ryckebusch, and T. Van Cauteren, Phys. Rev. C **73**, 045207 (2006).

[15] T. Corthals, T. Van Cauteren, J. Ryckebusch, and D. G. Ireland, Phys. Rev. C **75**, 045204 (2007).

[16] T. Corthals, T. Van Cauteren, P. Vancraeyveld, J. Ryckebusch, and D. G. Ireland, Phys. Lett. B **656**, 186 (2007).

[17] P. Vancraeyveld, L. De Cruz, J. Ryckebusch, and T. Van Cauteren, Phys. Lett. B **681**, 428 (2009).

[18] N. Phaisangittisakul, Ph.D. dissertation, University of California Los Angeles, 2001 [http://cbmaster.physics.ucla.edu/Crystalball/Docs/theses.html].

[19] T. D. S. Stanislaus *et al.*, Phys. Rev. C **79**, 015203 (2009).

[20] T. Van Cauteren, J. Ryckebusch, B. Metsch, and H. R. Petry, Eur. Phys. J. A **26**, 339 (2005).

[21] T. Van Cauteren, J. Ryckebusch, B. Metsch, and H. R. Petry, Eur. Phys. J. A **31**, 613 (2007).

[22] R. Manweiler *et al.*, Phys. Rev. C **77**, 015205 (2008).